American Mineralogist, Volume 93, pages 300–314, 2008

Prograde muscovite-rich pseudomorphs as indicators of conditions during metamorphism: An example from NW Maine

Barbara L. Dutrow,[1,*] C.T. Foster Jr.,[2] and Jennifer Whittington[1,†]

[1]Department of Geology and Geophysics, Louisiana State University, Baton Rouge, Louisiana 70803, U.S.A.
[2]Department of Geosciences, University of Iowa, Iowa City, Iowa 52242, U.S.A.

Abstract

During metamorphism, evidence of the prograde path is commonly obliterated by continued recrystallization as temperatures increase. However, prograde pseudomorphs that are common in many terrains may provide insight into this portion of the metamorphic path if their mineralogy can be accurately interpreted. Seventeen sillimanite-zone metapelitic samples, each containing 2–5 muscovite-rich pseudomorphs, from the Farmington Quadrangle, Maine, U.S.A., were investigated to evaluate their use as indicators of conditions during prograde metamorphism. SEM-CL images, X-ray maps, image analysis, and electron microprobe analyses characterize the mineral distribution, modes, and compositions within the pseudomorph and the surrounding matrix. Based on modal mineralogy determined from image analyses, the muscovite-rich pseudomorphs are divided into four major types: muscovite-rich (>70% muscovite), quartz-muscovite (60–70% muscovite with 10–25% quartz), plagioclase-muscovite (58–72% muscovite with 10–20% plagioclase), and sillimanite-plagioclase-muscovite (50–60% muscovite with 10–20% each plagioclase and sillimanite). A biotite-rich, muscovite-poor mantle surrounds many pseudomorphs. All pseudomorphs are interpreted to be prograde, based on their texture, and are after staurolite because of the partial replacement of staurolite by coarse muscovite at lower grades.

Textural modeling of reaction mechanisms required to reproduce the observed mineralogy in the pseudomorphs indicates that each major pseudomorph type holds clues to the prograde path and represents a different mechanism of formation. Muscovite-rich and quartz-muscovite pseudomorphs formed by the breakdown of staurolite containing different modal amounts of poikiloblastic quartz. Quartz-muscovite pseudomorphs likely reflect a quartz-rich initial rock composition. Plagioclase-muscovite pseudomorphs require the infiltration of Na-bearing fluids. Sillimanite-plagioclase-muscovite pseudomorphs require a two-stage process; the infiltration of Na-rich fluids during staurolite breakdown followed by sillimanite growth. The subtle mineralogical differences recorded in the pseudomorphs studied here provide evidence of previously unrecognized controls along the prograde path during metamorphism.

Keywords: Pseudomorph, metamorphism, diffusion, metapelites, reaction mechanisms

Introduction

As temperatures and pressures increase during metamorphism, mineral textures transform in response to the newly imposed conditions. These textural changes may be dramatic, as in the case of skarn formation (e.g., Johnson and Norton 1985), or they may be more subtle, as in the formation of pseudomorphs (e.g., Guidotti 1968). As such, textures when combined with mineralogy may provide insights into formation conditions of the rock (e.g., Dutrow et al. 1999; Guidotti and Johnson 2002).

Pseudomorphs are recognized in many metamorphic terranes (e.g., Guidotti 1968; Foster 1977; Cesare 1999a; Collier and Plimer 2002; Novák et al. 2004; Brady et al. 2004; cf. Ferry 2000), where they form in response to increasing temperatures (prograde pseudomorphs) or decreasing temperatures typically accompanied by fluid infiltration (retrograde pseudomorphs). Guidotti (1968) was the first to recognize that large segregations of muscovite found in metapelites in the Rangeley-Oquossoc areas of Maine were pseudomorphs. By tracing these textural features to lower grades, he demonstrated that these formed from the replacement of staurolite as temperatures increased along the prograde path into the sillimanite zone and interpreted their importance in recording metamorphic history. He further suggested that these segregations formed by a different reaction mechanism than those that form retrograde pseudomorphs (Guidotti 1968). In later studies (e.g., Guidotti 1970, 1974; Guidotti and Johnson 2002), he described evidence for the pseudomorphing process being constant volume limited by the bulk composition and that it closely approached chemical equilibrium.

Since Guidotti's original description, other workers have described muscovite-rich pseudomorphs from various localities, but none have completed detailed studies of their mineralogy. Grew and Day (1972) briefly described muscovite replacement of staurolite in the Narragansett Basin of Rhode Island, U.S.A.,

* E-mail: dutrow@lsu.edu
† Present address: EnCana Oil and Gas (U.S.A.), Inc., 14001 North Dallas Parkway, Dallas, Texas 75240, U.S.A. E-mail: jennifer.whittington@encana.com.

suggested that this was textural evidence for disequilibrium, and attributed this replacement to be the result of multiple metamorphic events. Muscovite production at the expense of staurolite was also described by Kwak (1974) for an andalusite-bearing rock from the Pyrenees, Spain. Through careful observation, he reasoned that the textural and chemical differences could be "partially attributed to the grains occurring in systems having different chemical environments during metamorphism" (p. 75). He developed two reactions to account for this texture, both requiring silica as a reactant. He further concluded that "Al during staurolite breakdown shows a significant mobility," that "areas of these textures must be considered to be open to significant element exchange," and that "each texture is a single equilibrium system" (p. 76). These observations led him to state that "metamorphic coronas...have different amounts (ratios) of product minerals, different product minerals and...reacted to different degrees or completion." Although he did not quantify this statement, his astute observations suggested local equilibrium, redistribution of minerals in a rock, element migration in local domains, and that chemical information is retained in the pseudomorphs and could be used to infer conditions during metamorphism.

More recently, Cesare (1999a, 1999b) noted the presence of "muscovite nodules" in a sample from the contact aureole of Vedrette di Ries pluton in the eastern Alps, Italy. These muscovite nodules contain staurolite inclusions that were interpreted to represent the prograde nature of the pseudomorph. He observed that muscovite had been redistributed to different sites throughout the rock. Based on matrix analysis of assemblages, he concluded that there is net consumption of phases but that prograde pseudomorphs of muscovite after staurolite can nevertheless occur, in keeping with Foster's earlier studies (e.g., Foster 1977).

These studies, based primarily on observation, highlight the different interpretations for the formation of prograde muscovite-rich pseudomorphs after staurolite; a single- or multiple-stage process in response to one or more metamorphic events. Thus, pseudomorphs may contain information on the prograde path or paths.

Evidence for the prograde path is commonly obliterated by continued recrystallization as temperatures rise. However, reaction mechanisms responsible for pseudomorph formation are recorded in the mineralogy of the prograde pseudomorphs and may provide detailed insight into conditions encountered during this portion of the metamorphic path. These mechanisms can be deciphered by quantitative analyses of mineral modes and chemistry in the pseudomorphs and the matrix when combined with irreversible thermodynamic modeling that constrains reaction mechanisms and local mass transport required for pseudomorph formation (e.g., Foster 1981, 1983; Dutrow et al. 1999).

As an example, quantitative studies of pseudomorphs from the Rangeley area in NW Maine, near the region of Guidotti's original work, significantly advanced the earlier descriptive work. Foster (1981) found that muscovite and biotite pseudomorphs after staurolite formed as a result of sillimanite nucleation that sets up chemical potential gradients between the growing sillimanite, pre-existing staurolite, and the rock matrix of biotite, muscovite, plagioclase, quartz, ilmenite, and garnet. Textural modeling studies of these pseudomorphs suggested that they form from mass transfer of approximately ten components between different domains of the rock via diffusion in a system closed to all components except H_2O. This leads to the pseudomorphing of staurolite by micas at the expense of the matrix phases (Foster 1977, 1983, 1986).

In a further quantitative study, irreversible thermodynamic modeling of reaction mechanisms was completed for tourmaline-bearing, muscovite-rich pseudomorphs from the nearby Farmington quadrangle, Maine (Fig. 1) to constrain their likely origin (Dutrow et al. 1999). That study suggested that pseudomorphs result from a three-stage process in a system open to infiltrating fluids: initially, muscovite partially replaced staurolite (Stage 1); the rocks were then infiltrated by B-rich fluids that triggered the nucleation and growth of tourmaline (Stage 2); and lastly, sillimanite nucleated and grew throughout the rock while staurolite continued to break down (Stage 3; Dutrow et al. 1999). In each of these quantitative analyses, reaction mechanisms recorded by the prograde pseudomorphs could be identified. Additionally,

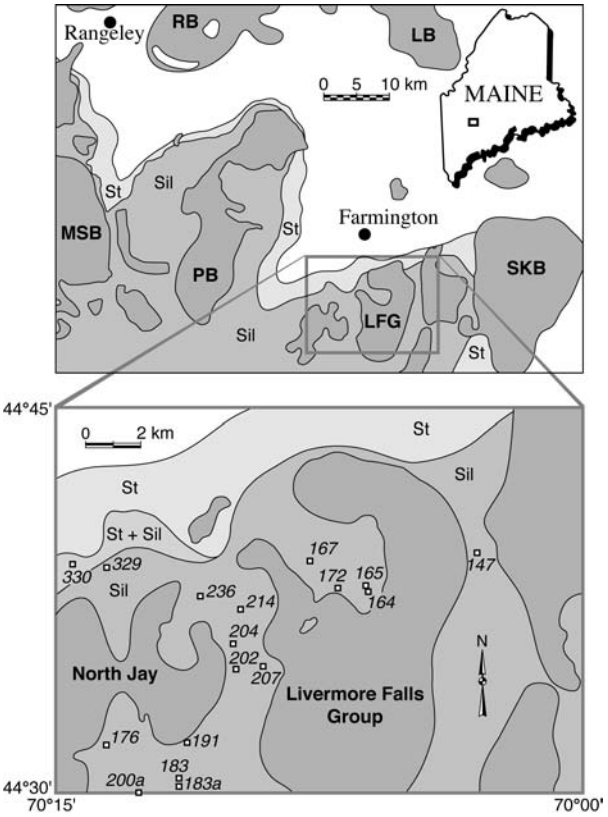

FIGURE 1. Metamorphic map of west-central Maine. Black dots locate the towns of Farmington and Rangeley (upper left corner). Plutons are dark gray: RB = Reddington Batholith, LB = Lexington Batholith, MSB = Mooselookmeguntic Batholith, PB = Phillips Batholith, LFG = Livermore Falls Group, SKB = Skowhegan Batholith. A solid box bounds the southern portion of the Farmington quadrangle enlarged in the lower diagram. Isograds increase in grade from NE to SW in the Farmington region and mark the first appearance of the mineral in the M_3 zones (upper and lower diagrams): Staurolite (St), St + sillimanite (Sil), and Sillimanite zones. Study samples (numbers) and locations (boxes) are within the sillimanite zone except for 330, which occurs in the transition zone (adapted from Dutrow 1985; Guidotti and Holdaway 1993; Dutrow et al. 1999).

these studies demonstrated that prograde pseudomorphs contain information on the metamorphic event.

The study reported here focuses on the use of a variety of muscovite-rich pseudomorphs from sillimanite-grade metapelites to test their utility as recorders of conditions along the prograde path. An ideal setting for this is in the Farmington quadrangle of west-central Maine where the well-equilibrated rocks contain abundant pseudomorphs of similar grade but with varying mineral modes (Dutrow 1985).

GEOLOGIC SETTING

Samples for this study were collected from metapelitic lithologies in the southern half of the Farmington quadrangle of west-central Maine (Fig. 1). The metamorphic history of this area is well-documented (e.g., Holdaway et al. 1988; DeYoreo et al. 1989; Guidotti et al. 1996) and only a short synopsis of events relevant to these samples is presented here.

West-central Maine underwent multiple mid-Paleozoic metamorphic episodes (M_1-M_3) that were closely spaced in both time and intensity (e.g., Holdaway et al. 1988; Guidotti 1989; Dutrow et al. 1999). The emplacement of numerous sheet-like granitoid intrusives of the Devonian New Hampshire Magma Series triggered metamorphism (e.g., Moench and Zartman 1976; Holdaway et al. 1988). In the Farmington area, only two events, M_2 and M_3, can be easily distinguished. M_2 is a widespread lower-pressure event that produced andalusite-staurolite assemblages in the metapelites. In the northwestern portion of the Farmington quadrangle, M_2 is recognized primarily as retrograde pseudomorphs of chlorite after staurolite or garnet that can be used to define N-S trending isograds (Dutrow 1985). These isograds are truncated by E-W trending isograds associated with the culmination of M_3 thermal events (394–379 Ma) that produced prograde garnet- through sillimanite-bearing assemblages at near isobaric conditions in the southern portion of the Farmington quadrangle while retrograding assemblages to the north (refer to Fig. 1; Dutrow 1985; Guidotti and Holdaway 1993; Dutrow et al. 1999). Although M_3 is regional in character with grade increasing to the south, isograds display a rough coincidence with exposed intrusive contacts (regional-contact metamorphism). Recrystallization during M_3 closely approached chemical equilibrium based on systematic element partitioning among the minerals and their textural relationships (Guidotti 1970; Guidotti and Holdaway 1993; Guidotti et al. 1996; Guidotti and Johnson 2002).

Metasediments of the Sangerville Formation are the dominant lithology that crops out in the Farmington area. These are primarily clastic and carbonate sediments of Silurian age (Pankiwskyj et al. 1976; Moench and Pankiwskyj 1988). The metasedimentary units trend NE-SW and the intrusives intersect the bedding at high angles. Samples in this study are predominantly from the metapelitic units.

The pseudomorph samples were collected from the M_3 sillimanite zone of the Farmington quadrangle that lies in a region of increasing metamorphic grade (e.g., Holdaway et al. 1982, 1988; Dutrow 1985; Guidotti and Holdaway 1993; Guidotti et al. 1996). As metamorphic grade increases, the fabric of the rock coarsens, schistosity increases, and chlorite disappears (e.g., Guidotti and Johnson 2002). The staurolite zone contains large (1.0–2.0 cm) poikiloblastic staurolite. Muscovite replacement of staurolite becomes more prominent approaching the sillimanite zone, as the staurolite becomes unstable concurrent with the nucleation and growth of sillimanite. Increasing temperatures near the sillimanite (Sil) zone trigger the breakdown of staurolite (St) in a biotite (Bt)-muscovite (Ms)-quartz (Qtz)-plagioclase (Pl)-garnet (Grt) matrix that is indicated by the whole rock net reaction (after Holdaway et al. 1988; Foster 1999):

$$St + Ms + Qtz \rightarrow Sil + Bt + Grt + H_2O \quad (1)$$

(abbreviations after Kretz 1983). This leads to a staurolite + sillimanite transition zone where both staurolite and sillimanite coexist (Fig. 1). As Guidotti (1968) observed, muscovite segregations could be traced from the sillimanite zone downgrade into the staurolite zone where incipient replacement of staurolite by coarse, randomly oriented muscovite could be seen as a muscovite rim around staurolite. In the transition zone, small amounts of staurolite remain in muscovite clots, whereas in the sillimanite zone only muscovite clots exist. A concomitant increase in sillimanite, as the amount of staurolite decreases upgrade within the transition zone, suggests that the development of the pseudomorphs is related to reaction 1 (Guidotti 1968, 1970). Thus, pseudomorphs in this study are interpreted to be after staurolite and to be prograde.

The Farmington pseudomorphs are composed of large, coarse, and randomly oriented muscovite grains, that also retain a morphology consistent with staurolite, providing additional evidence that they are prograde. In contrast, retrograde staurolite pseudomorphs are composed of a lower temperature mineral assemblage, such as chlorite and muscovite, and are finer grained (e.g., Holdaway et al. 1988). Both retrograde and prograde pseudomorphs have crystal forms that indicate near constant volume replacement.

Temperatures for the M_3 sillimanite zone are estimated to be near 580 ± 25 °C based on biotite-garnet geothermometry (Dutrow 1985; Holdaway et al. 1988) and 580 to 650 °C for these pseudomorphs based on the Ti-in-biotite geothermometry (Henry et al. 2005; reported in Whittington 2006). The highest temperature, 650 ± 10 °C, was determined from biotite in the pseudomorph of sample 183a. This sample is located near the southern edge of the Farmington quadrangle, which is well within the upper sillimanite zone (Fig. 1). The lowest temperature, 580 ± 21 °C, was determined from the biotite in the pseudomorph of sample 329, collected from the sillimanite zone but near the boundary with the staurolite zone (Fig. 1). The average temperature calculated using Ti in biotite from the pseudomorphs and matrix is 623 ± 28 °C. Pressures of 3.25 ± 0.25 kbar are calculated from muscovite-almandine-biotite-sillimanite (MABS) geobarometry and from phase relations (Holdaway et al. 1988).

METHODS

Analytical techniques

Polished thin sections of 40 metapelitic samples collected from the sillimanite zone of the Farmington quadrangle (Fig. 1) were examined using light microscopy to select pseudomorphs with discernible boundaries and to identify those with contrasting mineral modes. Seventeen samples, each containing 2–5 pseudomorphs, were analyzed further to identify mineral phases, determine modal mineralogy and mineral distribution, and quantitatively characterize mineral chemistry (see Appendix 1). All pseudomorph samples contain >50% muscovite and ≤2% each

garnet and tourmaline. Most samples contain garnet in the matrix, but only two samples contain garnet inside the pseudomorph boundary.

The scanning electron microscope (SEM) model JEOL JSM-840A at Louisiana State University was used to quantify mineral modes via image analysis. Images collected include digital back-scattered electron images (BSE), elemental distribution (X-ray) maps, and cathodoluminescence (SEM-CL) images. X-ray maps provided the basis for image analyses. X-ray maps were obtained by energy dispersive spectroscopy (EDS) using a Tracor Northern microtrace EDS detector. An accelerating potential of 20 kV, a beam current of 10–20 nA, and a 1–2 μm focused electron beam were used. A 16-bit grayscale (256 shades) digital image (5.75 mm) was produced for each element. The elements Si, Al, K, Fe, Na, Ca, Ti, Mg, Mn, and P were selected for mapping because all the major mineral phases can be discriminated by a combination of these elements.

Individual element X-ray maps were combined into a composite image using an RGB color scheme by the image-processing program ImageJ (Rasband 1997). Because the composite image was developed from combined elemental maps using actual X-ray counts for each mineral in each sample, differences in chemical abundance of the elements resulted in slightly different colors for the same minerals between samples, e.g., greenish-brown vs. brownish-green. With composite X-ray maps, all mineral phases could be identified. This was essential for quartz and plagioclase, important components of the pseudomorphs, which could not be distinguished easily using optical microscopy or BSE. Details for the cathodoluminescent images and wavelength dispersive electron microprobe analyses are given in Appendix 1.

Calculation of modes

Modal amounts of muscovite, biotite, plagioclase, quartz, sillimanite, and ilmenite within the pseudomorphs and matrix were calculated using area percentages determined by analysis of 16-bit grayscale (256-shade) BSE and X-ray maps. Although these modes were determined for two-dimensional slices, the mineral grain size and distribution are not expected to be substantially different in three dimensions. The pseudomorph image area was selected and isolated using Adobe Photoshop, ensuring that pseudomorph modes would not be influenced by the surrounding matrix modes. The Al X-ray map proved useful for modal analysis because the mineral phases of interest each contain distinctive amounts of Al, and therefore, each mineral can be distinguished by a different shade of gray. The threshold function of the image-processing program ImageJ (Rasband 1997) distinguishes a mineral phase based on its assigned gray level of the 256-shade scale and then calculates the area of the phase. The modal percentage of that mineral was then normalized to the total area of the pseudomorph. The same magnification was used for all the BSE and X-ray images. The modes calculated from both X-ray and backscattered electron images differed by ±2%.

Textural modeling

Mineral reaction mechanisms responsible for pseudomorph formation were determined by irreversible thermodynamic models (Fisher 1977) of local reactions and material transport using the textural modeling program SEG (Foster 1993), which performs the calculation procedure described by Foster (1981). This approach combines material transport equations, conservation equations, and Gibbs-Duhem equations at constant T and P to calculate the reaction mechanisms that develop in a rock under a system of local equilibrium (see Appendix 2 for details). This technique has been used to explain a wide variety of textures in upper amphibolite-facies metapelites (Foster 1981, 1982, 1983, 1986, 1990, 1991, 1999; Dutrow et al. 1999).

Assumptions used in the calculations are that (1) the system is in local equilibrium; (2) the mineral compositions and relative diffusion coefficients are constant for a single model; (3) the system is open to H_2O-rich fluids and saturated with the fluid along grain boundaries; and (4) the system remains at steady state because compositional changes of the fluids along the grain boundaries are negligible (Foster 1981).

Input data for the modeling studies (Appendix 2) include mineral compositions (Table 1), mineral modes (Table 2), and relative diffusion coefficients (Table 3). Mineral compositions for biotite, muscovite, and plagioclase used in the modeling for this study were determined from electron-microprobe analyses (Whittington 2006); the staurolite composition was taken from electron-microprobe data of Farmington rocks reported in Dutrow (1985). Mineral modes of representative pseudomorphs were developed from image analyses (Table 2). Relative diffusion coefficients used in this study (Table 3) were taken from Foster (1981) except for that of SiO_2, which is from Foster (1990). Oxide components are used because speciation in pelitic grain-boundary fluids is not well understood at these temperatures and pressures. The relative diffusion coefficients were derived from Rangeley, Maine metamorphic rocks (see also Discussion) and should be valid for modeling the Farmington area pseudomorphs because of the similarities in P-T conditions and bulk compositions.

TABLE 1. Mineral compositions used in the textural modeling (in apfu)

Muscovite	Ms	$K_{0.79}Na_{0.16}Al_{2.87}Fe_{0.05}Mg_{0.05}Ti_{0.03}Si_{3.03}O_{10}(OH)_2$
Biotite	Bt	$K_{0.88}Na_{0.05}Fe_{1.33}Mg_{0.98}Ti_{0.09}Al_{1.79}Si_{2.68}O_{10}(OH)_2$
Plagioclase	Pl	$Na_{0.77}Ca_{0.22}Al_{1.22}Si_{2.78}O_8$
Staurolite*	St	$Fe_{3.54}Mg_{0.57}Al_{17.79}Ti_{0.10}Si_{7.64}O_{48}H_{3.38}$
Sillimanite	Sil	Al_2SiO_5
Quartz	Qtz	SiO_2

* St data from Dutrow (1985); Mn minor, F, Cl in micas below detection; abbreviations after Kretz (1983).

RESULTS

Sample description

Muscovite-rich pseudomorphs occur in sillimanite zone metapelitic schists with a matrix assemblage consisting of approximately 30% biotite, 29% quartz, 20% muscovite, 9% sillimanite, 8% plagioclase, and 1% ilmenite ± garnet ± tourmaline ± apatite ± graphite based on calculated modal amounts; actual modes vary among the samples (Table 2). Sillimanite occurs as fibrolitic mats typically in radial clusters or as clumps with filament-like tails that crosscut pseudomorphs. These mats are commonly proximal to biotite clusters (Foster 1991). Euhedral crystals of sillimanite are found in one sample (172a), where they occur in the center of the pseudomorph, in contrast to the fibrolitic sillimanite that is concentrated in the mantle area and immediately inside the pseudomorph boundary. Small fibrous sillimanite grains occur as inclusions in plagioclase in the plagioclase-rich and sillimanite-poor rocks. Samples with greater amounts of plagioclase have distinctly less sillimanite, and conversely, samples with abundant sillimanite have less plagioclase. Quartz veins are present in four of the seventeen samples. Matrix foliation wraps around the pseudomorphs and mantle areas (Fig. 2).

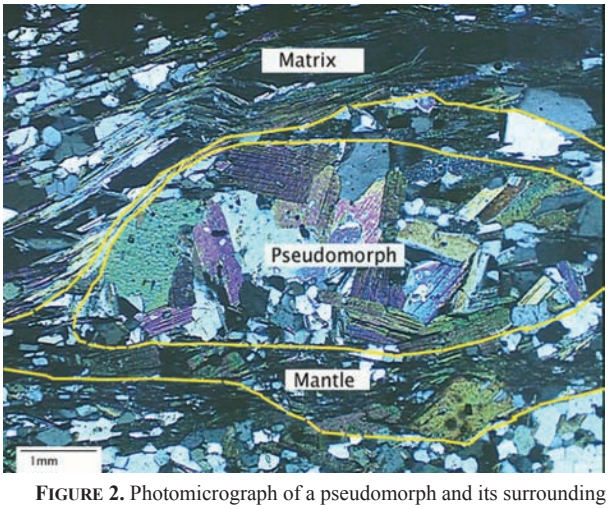

FIGURE 2. Photomicrograph of a pseudomorph and its surrounding region (cross-polarized light; sample 330). The pseudomorph displays the characteristic ovoid shape, change in modal mineralogy, and the random orientation and coarse grain size of muscovite relative to that in the matrix. The mantle mimics the shape of the pseudomorph and is rich in biotite and plagioclase. Matrix minerals are biotite, muscovite, quartz, and plagioclase.

Many pseudomorphs are separated from the matrix by a mantle region (1–2 mm thick) that closely follows the shape of the pseudomorph but differs in modal mineralogy. The mantle is typically enriched in biotite and plagioclase and may contain minor muscovite, quartz, and sillimanite. Elongate micas are oriented parallel to pseudomorph boundary (Fig. 2).

The muscovite-rich pseudomorphs range in size from 3.0 mm to 1.6 cm. They are easily distinguished in hand specimen by their ovoid shape and the high concentration of large muscovite laths that imparts a light color to the pseudomorphs in the darker, biotite-rich matrix. Guidotti (1968) referred to these segregations as "spangles." Two samples contain pseudomorphs greater than 1.5 cm in size and have a more rounded shape. In thin section, pseudomorphs are characterized by a change in modal mineralogy to coarse-grained muscovite aggregates (individual grain size 3.0–6.0 mm). These muscovites have a distinctly different grain size than matrix muscovites (1.0 mm). The randomly oriented, coarse muscovite flakes are oblique to matrix foliation (Fig. 2) suggesting that staurolite replacement was a post-tectonic event. Some pseudomorphs contain additional minor mineral phases (Table 2).

TABLE 2. Mineral modes (%) calculated for the pseudomorphs (ps) and matrix (mtx) by image analysis (±2%)

	Quartz-muscovite									
	330		176		165		147		164	
	ps	mtx	ps	mtx	ps	mtx	ps	mtx	ps	mtx
Ms	60	28	58	27	70	24	67	19	68	16
Bt	7	26	15	33	15	33	17	29	12	32
Pl	1	8	8	6	2	6	2	10	2	4
Sil	1	6	5	19	0	4	0	3	5	15
Qtz	25	25	17	12	13	25	12	31	12	22
Ilm	2	4	1	2	1	3	1	3	tr	3
Ap	tr	1	3	0	tr	2	tr	2	1	2
Grt	0	2	0	4	1	4	0	3	1	6
	Muscovite-rich									
	183		236		200a		191		202	
	ps	mtx	ps	mtx	ps	mtx	ps	mtx	ps	mtx
Ms	80	22	75	25	70	20	70	32	70	33
Bt	7	32	8	25	8	31	10	27	10	20
Pl	3	10	0	5	6	10	7	5	7	10
Sil	2	10	8	15	4	12	3	10	6	12
Qtz	1	18	6	20	1	20	5	16	4	20
Ilm	1	2	5	3	1	2	4	3	1	2
Ap	2	3	1	2	2	3	2	4	2	3
Grt	0	3	0	5	0	4	0	3	0	4
	Plagioclase-muscovite									
	207		183a		329		204			
	ps	mtx	ps	mtx	ps	mtx	ps	mtx		
Ms	58	19	72	13	60	25	64	29		
Bt	8	26	7	27	5	27	12	21		
Pl	22	17	18	31	16	18	12	13		
Sil	5	5	0	2	2	2	5	11		
Qtz	6	25	2	25	13	20	3	18		
Ilm	1	4	0	1	5	4	2	3		
Ap	tr	2	1	3	1	1	1	2		
Grt	0	2	0	0	0	2	0	5		
	Sillimanite-plagioclase-muscovite									
	172a		167		214					
	ps	mtx	ps	mtx	ps	mtx				
Ms	50	20	60	15	58	23				
Bt	6	28	7	20	12	21				
Pl	20	12	12	17	10	17				
Sil	21	14	12	12	12	9				
Qtz	2	24	8	30	5	22				
Ilm	tr	1	tr	3	1	3				
Ap	tr	1	tr	1	2	2				
Grt	0	2	0	3	0	3				

Notes: Samples are listed according to mineral abundance for the identifying minerals of that pseudomorph type (refer to text for explanation on pseudomorph types). tr = trace amount.

Pseudomorph types

A range of modal mineralogy, as calculated from image analyses, is observed in pseudomorphs from the 17 samples (Table 2). All pseudomorphs contain at least 50% muscovite with varying and lesser amounts of biotite, plagioclase, quartz, and sillimanite. Depending on the relative amounts of these minerals, pseudomorphs could be grouped into four major types. These are: quartz-muscovite, muscovite, plagioclase-muscovite, and sillimanite-plagioclase-muscovite pseudomorphs. All pseudomorphs analyzed within a single sample belong to the same pseudomorph type (Fig. 3) and have similar mineral modes (Table 4). Therefore, intrasample variability was limited.

Quartz-muscovite pseudomorphs contain up to 25% quartz, the most observed in any pseudomorph type, in addition to muscovite (58–70%), lesser biotite (7–17%), and <8% each plagioclase and sillimanite (Fig. 4a; Table 2; $n = 5$). This type of pseudomorph ranges in size from 3.0 to 6.0 mm and has mantles that are only partially developed. Based on CL images of these pseudomorphs (samples 147, 330), sillimanite is more abundant within the matrix (3–19%) than the pseudomorphs (1–5%). In addition, samples with more sillimanite in the matrix (19%) contain more sillimanite in the pseudomorphs (5%). In these rocks, sillimanite is observed as fibrolitic needles in both the matrix and pseudomorphs, but it also occurs as clusters of coarse grains in the matrix.

The muscovite pseudomorphs contain the most muscovite, relative to other pseudomorph types, with a mode of ≥70% muscovite and only minor amounts of other phases, <10% each plagioclase, sillimanite, and biotite (Fig. 4b; Table 2; $n = 5$). This is in stark contrast to the matrix that consists of only 22% muscovite but abundant biotite, plagioclase, and quartz (~20% each). Modes of sillimanite and plagioclase appear to be the most variable in this pseudomorph type. The mantle region is typically enriched in biotite and plagioclase but some samples lack a well-developed mantle.

Plagioclase-muscovite pseudomorphs are characterized by larger amounts of plagioclase, up to 22%, in addition to muscovite

TABLE 3. Relative diffusion coefficients used in this study (from Foster 1981, 1990)

FeO	$NaO_{1/2}$	MgO	$AlO_{3/2}$	SiO_2	$KO_{1/2}$	CaO	TiO_2
2.63	0.93	1.82	5.88	5.0	1.0	0.17	0.38

TABLE 4. Mineral modes of two pseudomorphs in a single sample (183a; Fig. 3); ±2%

	Plagioclase-muscovite			
	Pseudomorph 1		Pseudomorph 2	
	ps	mtx	ps	mtx
Ms	72	13	67	13
Bt	7	27	10	27
Pl	18	31	22	31
Sil	0	2	0	2
Qtz	2	25	1	25
Ilm	0	1	0	1
Ap	1	3	0	3
Grt	0	0	0	0

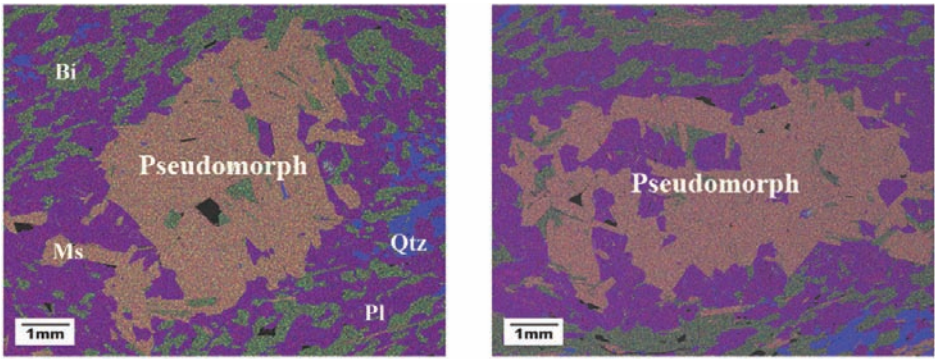

FIGURE 3. Composite X-ray images showing two muscovite-rich pseudomorphs from the same thin section (183a) with similar mineral modes. Elements are Na + Ca + K + Fe + Si + Al. Colors represent the same mineral in each image. (See Table 1 for mineral abbreviations.)

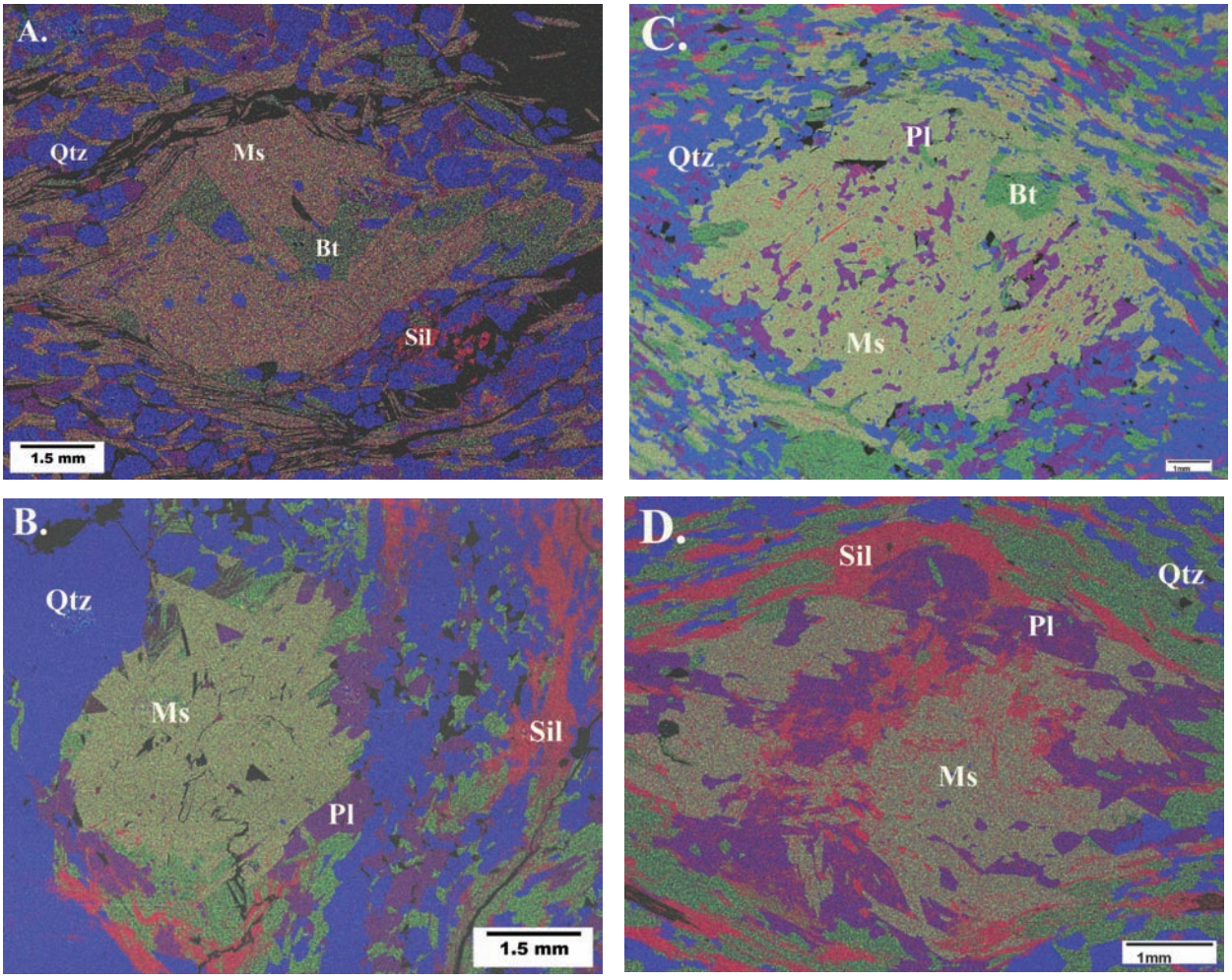

FIGURE 4. Four types of mica pseudomorphs found in the study area as shown by composite X-ray images. Slight color variations reflect differences in X-ray counts. Brown to brownish green = Ms; bright green = Bt; blue = Qtz; purple = Pl; red = Sil. (See Table 2 for calculated modes.) (**a**) Quartz-muscovite pseudomorph (sample 147). The pseudomorph contains ~30% Qtz in addition to 67% Ms. Black is an epoxy-filled fracture filled. (**b**) Muscovite pseudomorph (sample 200). This pseudomorph contains 80% Ms, 7% Bt, 3% Pl, 2% Sil, and 1% Qtz and is surrounded by a mantle rich in biotite (bright green). Matrix contains greater amounts of Bt, Ms, Qtz, and Pl. (**c**) Plagioclase-muscovite pseudomorph (sample 207). This pseudomorph contains 58% Ms, 22% Pl, 8% Bt, 6% Qtz, 5% Sil, and 1% Ilm compared to the matrix with less Pl and more Bt and Qtz. Mantle is absent. Plagioclase in this pseudomorph retains an earlier foliation. (**d**) Sillimanite-plagioclase-muscovite pseudomorph (sample 172a). This pseudomorph contains 20% Sil and 20% Pl in addition to 50% Ms. The mantle contains biotite and lacks quartz while the matrix contains 24% Qtz and 28% Bt. Fibrolitic sillimanite is present in the pseudomorph and mantle.

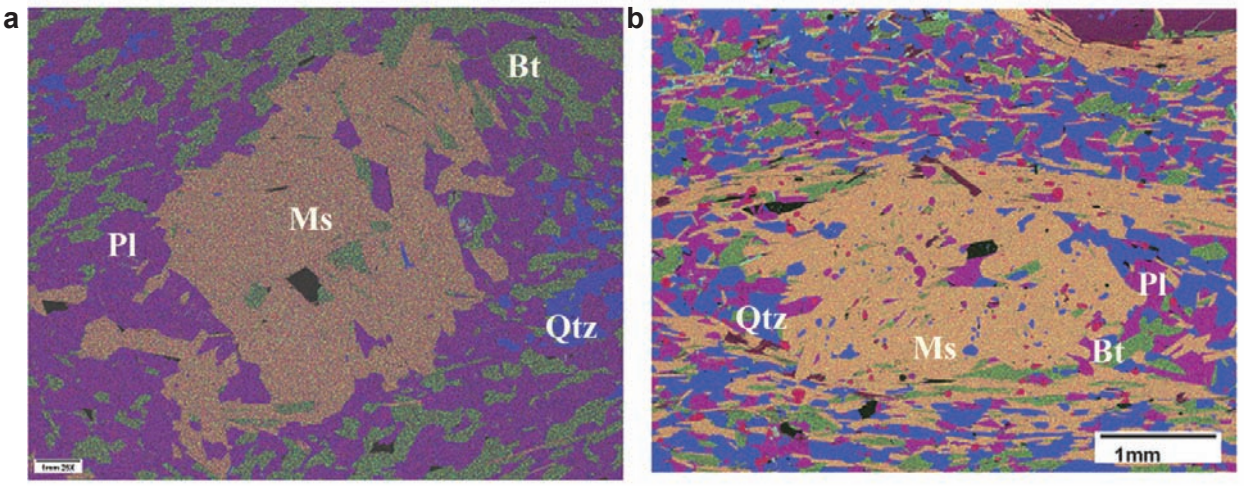

FIGURE 5. Composite X-ray image of two plagioclase-muscovite pseudomorphs from different samples—183a (**a**), 329 (**b**)—with similar modal mineralogy. See also Figure 4c (sample 207). Color variations for muscovite result from slightly different X-ray counts when creating composite images.

(58–72%) with <10% each biotite, quartz, and sillimanite (Fig. 4c; Table 2; n = 4). These pseudomorphs and the surrounding matrix contain the highest modal amount of plagioclase within the pseudomorphs and matrices, variable amounts of muscovite, and the least amount of sillimanite. Three plagioclase-muscovite pseudomorphs from different samples display similar modal mineralogy (Figs. 4c and 5; Table 2). The mantle in some samples is not well-defined. Less than 1% quartz was observed inside the pseudomorph, and small individual needle-like grains of sillimanite (not fibrolite mats) were restricted to the mantle area outside the pseudomorph. In CL, sample 183a shows an abundance of light blue luminescent plagioclase in the pseudomorph and surrounding matrix. Plagioclase is also more abundant in the matrix than in the pseudomorph. Optical examinations underestimated the modal amount of plagioclase within the pseudomorphs because it was mistaken for quartz. Using both X-ray and CL images, plagioclase modes were determined to be much higher.

Sillimanite-plagioclase-muscovite pseudomorphs contain abundant plagioclase (10–20%) and sillimanite (10–21%) in addition to muscovite (50–60%), with <12% each quartz and biotite (Fig. 4d). This type of pseudomorph contains the highest modal amount of sillimanite. Sillimanite is both fibrolitic and prismatic and is easily recognized by its bright red luminescence in CL (Fig. 6). These pseudomorphs are surrounded by a quartz-free, biotite- and sillimanite-rich mantle and occur in a quartz-muscovite-rich and plagioclase-poor matrix (Table 2).

Mineral chemistry

Seven samples were analyzed with the electron microprobe (EMPA) to establish the chemical composition of muscovite, biotite, and plagioclase within the pseudomorph and the matrix (Table 1). In addition to those elements given in Table 1, muscovite and biotite contain <0.007 and <0.02 apfu Mn, respectively, <0.015 apfu Ba, and F and Cl were below detection limits. Staurolite contains <0.04 apfu Zn. Because Mn was minor in all phases, it was not considered in the subsequent modeling studies. The chemical composition of the matrix biotite, muscovite, and plagioclase are similar to the compositions of those minerals in the pseudomorph in each sample. Element partitioning suggests an approach to chemical equilibrium; Mg/Fe ratios for samples containing coexisting biotite in the pseudomorph (0.419–0.472) and biotite in the matrix (0.419–4.61) plot along a straight line (Whittington 2006). Na/(K + Na) values in muscovite from the matrix and pseudomorph also indicate consistent element partitioning (Whittington 2006). Both pseudomorph and matrix muscovite have a small and similar amount of Na substitution for K (paragonite content), ranging from 0.21–0.34 apfu. The Fe_{tot} values in the muscovite (0.118–0.130 apfu) and biotite (2.045–2.894 apfu) are similar to other analyses for sillimanite zone metapelites of the Rangeley quadrangle (Guidotti 1973). Titanium levels in the biotite range from 0.258 to 0.330 apfu, sufficient amounts for using the Ti-in-biotite geothermometer.

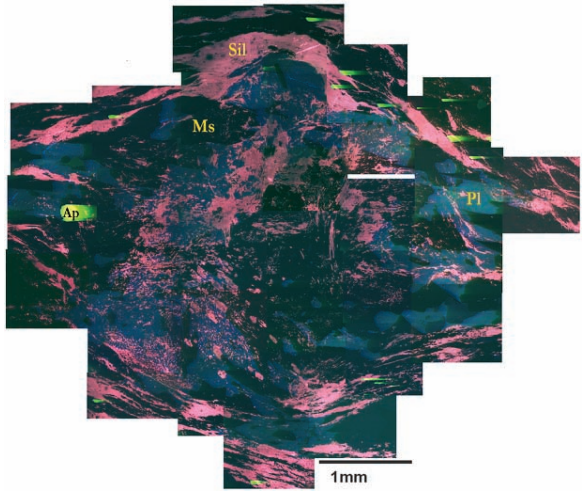

FIGURE 6. CL image of sample 172a with a sillimanite-plagioclase-muscovite pseudomorph showing the abundance of Sil (red), Pl (blue), and apatite (yellow). The fibrolitic sillimanite wraps around and penetrates the pseudomorph. Coarse sillimanite is present within the pseudomorph.

Feldspar grains within the pseudomorphs of most samples are Na-rich plagioclase, $Ab_{63.0–96.0}$ (andesine-albite). Feldspar in one sample (147) is albitic in the center of the grain and more potassium-rich near the rims.

Analysis of quartz in the quartz-muscovite pseudomorphs detected trace amounts of Al, ranging from ~200 ppm near the rims and ~100 ppm toward the centers of the grains. Titanium was also detected, levels ranged from 44 ppm at the rim to 27 ppm at the core. Due to the large errors associated with these analyses, the Ti-in-quartz thermometer was not used.

Pseudomorph reaction mechanisms

Reaction mechanisms responsible for each pseudomorph type were determined by textural modeling. Using mineral chemistry (Table 1) and calculated mineral modes (Table 2) for a representative of each pseudomorph type and its surrounding matrix, thermodynamic models of mineral textures were used to determine the mass transport and likely reaction mechanisms responsible for pseudomorph formation under conditions of local equilibrium (Appendix 2).

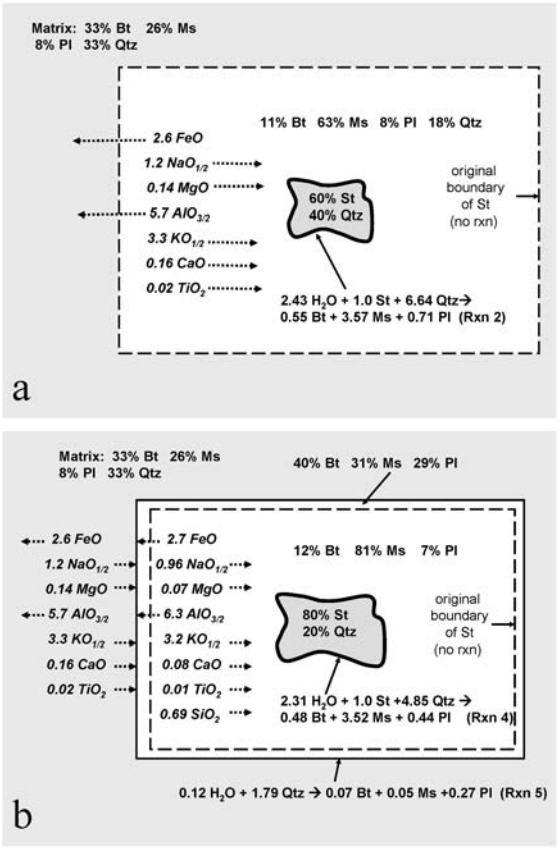

Figure 7. Schematic diagram showing the morphology, mineral modes, local reactions, and material transport for the formation of various pseudomorphs after staurolite (shown in Fig. 4) as described in the text. (**a**) Quartz-muscovite pseudomorph formed by reaction 2. (**b**) Quartz-free muscovite pseudomorph formed by reactions 4 and 5. (**c**) Muscovite pseudomorph formed from reactions 6 and 7. (**d**) Plagioclase-muscovite pseudomorph formed by reaction 8. (**e**) Sillimanite-plagioclase-muscovite pseudomorph. Late sillimanite formed in a pre-existing pseudomorph formed by reactions 9 and 10.

Quartz-mica and muscovite-rich pseudomorphs. When staurolite is consumed under local equilibrium conditions in a matrix of muscovite, biotite, plagioclase, and quartz, the Gibbs-Duhem constraints on transport through the matrix cause the reaction to consume staurolite and quartz and to produce muscovite, biotite, and plagioclase (Foster 1981). For the mineral compositions (Table 1) and relative diffusion coefficients (Table 3) in this study, the resulting reaction among the phases is

$$2.43\ H_2O + 1.0\ St + 6.64\ Qtz \rightarrow 0.55\ Bt + 3.57\ Ms + 0.71\ Pl. \quad (2)$$

Reaction 2 also consumes Na, Mg, K, Ca, and Ti that is supplied by diffusion through the matrix surrounding the staurolite

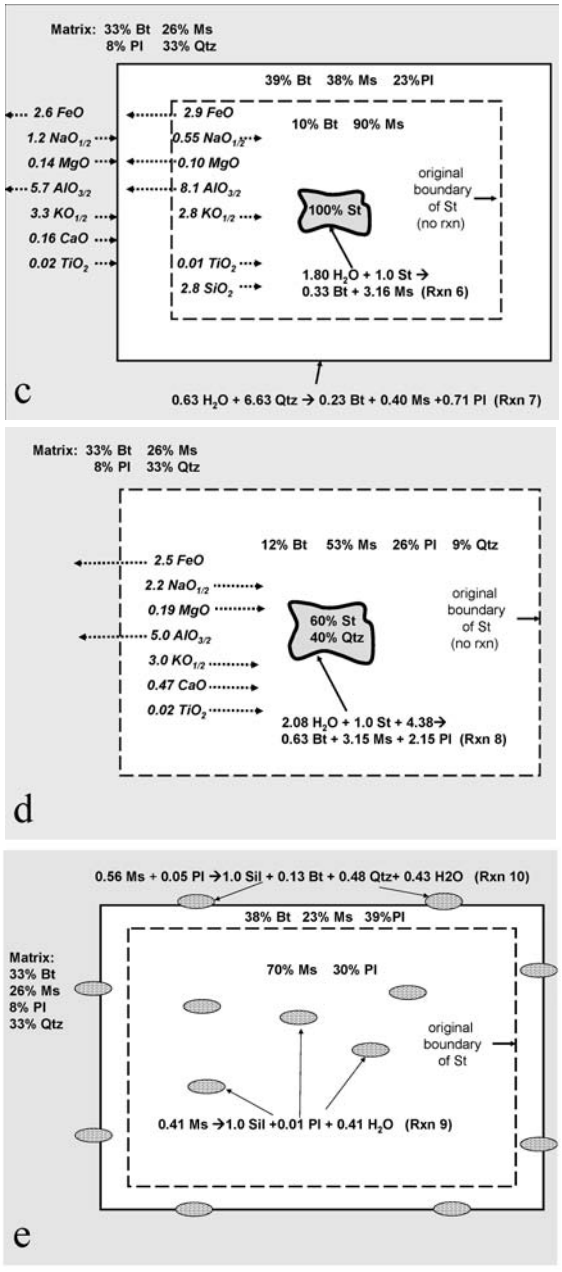

and produces Fe and Al, which are removed by diffusion through the matrix (Fig. 7a). If the staurolite is poikiloblastic and contains sufficient quartz to supply the amount needed by reaction 2, the modeled pseudomorph consists of muscovite, biotite, and plagioclase in a volume ratio of about 6:1:1. If the poikiloblast contains more than about 25% quartz, the excess will remain in the pseudomorph. For example, a poikiloblast with 60% staurolite and 40% quartz would produce a pseudomorph containing 63% muscovite, 11% biotite, 8% plagioclase, and 18% quartz (Fig. 7a). The muscovite, biotite, and plagioclase are formed by reaction 2 and the quartz is the amount of excess poikilitic quartz that remains after the staurolite is consumed. The end product is a quartz-muscovite pseudomorph (Fig. 4a).

If the amount of quartz contained in the staurolite is not sufficient to supply all of the quartz needed for reaction 2, some silica must be supplied by diffusion through the pseudomorph grain boundaries from quartz consumption in the matrix. In this situation, the reacting staurolite poikiloblast produces a quartz-free muscovite-rich pseudomorph via a reaction such as

$$1.98\ H_2O + 1.0\ St + 0.29\ Pl \rightarrow 0.29\ Bt + 3.38\ Ms \quad (3)$$

or

$$2.31\ H_2O + 1.0\ St + 4.85\ Qtz \rightarrow 0.48\ Bt + 3.52\ Ms + 0.44\ Pl. \quad (4)$$

Reaction 3 consumes Na, Si, and K that are supplied by diffusion through the pseudomorph surrounding the staurolite and it produces Fe, Mg, Al, Ca, and Ti, which are removed by diffusion through the pseudomorph. Reaction 4 consumes Na, Mg, Si, K, Ca, and Ti, which are supplied by diffusion through the pseudomorph surrounding the staurolite, and it produces Fe and Al, which are removed by diffusion through the pseudomorph (Fig. 7b). The amount of poikilitic quartz available in the staurolite poikiloblast is the controlling factor that determines the exact stoichiometry of reactions 3 and 4. Reaction 3 describes the situation where there is no poikilitic quartz and reaction 4 is for the situation where there is 20% poikilitic quartz.

The silica required to balance reactions 3 and 4 is supplied by grain boundary diffusion that is driven by the chemical potential gradient in the pseudomorph surrounding the remaining staurolite. The chemical potential gradient of SiO_2 in the pseudomorph produced by reaction 3 is approximately 3.5 times larger than the gradient for reaction 4 because the amount of silica necessary to balance reaction 3 that has to diffuse through the pseudomorph is 3.5 times larger than needed to balance reaction 4, due to the availability of poikilitic quartz at the reaction site for reaction 4. The difference in the silica gradient also affects all of the gradients for other components because of the Gibbs-Duhem relationships of the phases that compose the pseudomorph (Appendix 2). The different gradients then affect the ability of constituents to diffuse through the pseudomorph to the reaction site, which changes the reaction stoichiometry.

An interesting result is that the amount of plagioclase consumed by reaction 3 will decrease as poikilitic quartz is increased in the staurolite until eventually plagioclase changes from a reactant to a product. Then the amount of plagioclase produced will continue to increase as the amount of poikilitic quartz is increased until there is sufficient quartz to supply all of the silica in reaction 2, which produces almost twice as much plagioclase as reaction 4. The pseudomorph produced by reaction 3 has a mode of 91% muscovite and 9% biotite and the pseudomorph produced by reaction 4 has a mode of 81% muscovite, 12% biotite, and 7% plagioclase (Fig. 7b). These are the types of reactions that produce the muscovite pseudomorphs (Fig. 4b) with little or no quartz and small amounts of biotite and plagioclase.

The silica required to balance reactions 3 and 4 comes from quartz consumption in the matrix at the margin of the pseudomorph via reactions that produce a biotite-plagioclase-rich mantle surrounding the pseudomorph. These reactions progress out into the matrix as the staurolite breaks down. The mantle thickness and mineral modes depend on the amount of poikilitic quartz in the original staurolite and the mineral modes in the matrix. A poikiloblastic staurolite with 20% quartz in the poikiloblast, reacting in a matrix of 33% biotite, 26% muscovite, 8% plagioclase, and 33% quartz will produce a mantle with a mode of 40% biotite, 31% muscovite, and 29% plagioclase (Fig. 7b) via the reaction:

$$0.12\ H_2O + 1.79\ Qtz \rightarrow 0.07\ Bt + 0.05\ Ms + 0.27\ Pl. \quad (5)$$

Reaction 5 consumes Fe, Na, Mg, Al, K, Ca, and Ti that are supplied by diffusion through the matrix and pseudomorph and it produces Si, which is removed by diffusion into the pseudomorph to provide the silica needed for reaction 4. If reactions 4 and 5 are combined they equal reaction 2. This is because the net reaction taking place in the mantle and pseudomorph is constrained by local equilibrium transport through the matrix around the developing mantle and pseudomorph, which is controlled by the same set of Gibbs-Duhem equations as in reaction 2.

If a staurolite poikiloblast has no or few quartz inclusions, the staurolite consuming reaction will be reaction 3. However, typically a staurolite without quartz inclusions also does not contain the necessary plagioclase required for reaction 3. In this case, the staurolite will be replaced by a pseudomorph containing 90% muscovite and 10% biotite (Fig. 7c) via the reaction:

$$1.80\ H_2O + 1.0\ St \rightarrow 0.33\ Bt + 3.16\ Ms. \quad (6)$$

Reaction 6 consumes Na, Si, and K that are supplied by diffusion through the pseudomorph surrounding the partially consumed staurolite and it produces Fe, Mg, Al, and Ti that are removed by diffusion through the pseudomorph (Fig. 7c). The mantle reaction that consumes quartz in the matrix at the edge of the pseudomorph to supply the silica necessary to balance reaction 6 is

$$0.63\ H_2O + 6.63\ Qtz \rightarrow 0.23\ Bt + 0.40\ Ms + 0.71\ Pl. \quad (7)$$

Reaction 7 consumes Fe, Na, Mg, Al, K, Ca, and Ti, which are supplied by diffusion through the matrix and pseudomorph, and it produces Si, which is removed by diffusion into the pseudomorph to provide the silica needed for reaction 6. Reaction 7 produces a mantle composed of 39% biotite, 38% muscovite, and 23% plagioclase that is about 3.5 times thicker than the mantle produced by reaction 5 because it consumes about 3.5 times more quartz in the matrix (cf. Figs. 7b and 7c). The mantle produced by reac-

tion 5 is most similar to the biotite-plagioclase mantles observed around muscovite-rich pseudomorphs in the Farmington area (Fig. 4b), suggesting most of the muscovite pseudomorphs are replacing staurolite with 20 to 25% poikilitic quartz.

Plagioclase-muscovite pseudomorphs. The maximum amount of plagioclase that can be produced in a pseudomorph that has replaced staurolite in a matrix of muscovite + biotite + plagioclase + quartz that is open to H_2O at the hand-specimen scale is about 8%, as given by reaction 2. Plagioclase-muscovite pseudomorphs with larger amounts of plagioclase, such as those shown in Figure 4c, require substantially more Na than can be supplied if the relative diffusion coefficients of Foster (1981) are used. This finding suggests that the system is open to an advective supply of Na at the hand-specimen scale.

To test this hypothesis, the system was opened to an infinite supply of Na by fixing the chemical potential gradient of $NaO_{1/2}$ at zero and providing/removing the necessary amount of Na required for local reactions. This resulted in a pseudomorph composed of 12% biotite, 46% muscovite, 38% plagioclase, and 3% quartz for a staurolite poikiloblast with 60% staurolite and 40% quartz. The amount of plagioclase is about twice that observed in the plagioclase-muscovite type of pseudomorph, suggesting that the supply of Na was too high. A system in which there was a limited supply of advective Na, achieved by increasing the relative diffusion coefficient of Na, reproduces these pseudomorphs. A relative diffusion coefficient for $NaO_{1/2}$ of 4 produces a pseudomorph with 26% plagioclase, 53% muscovite, 12% biotite, and 9% quartz from a poiklioblast of 60% staurolite and 40% quartz (Fig. 7d) via the reaction:

$$2.08\ H_2O + 1.0\ St + 4.38\ Qtz \rightarrow 0.63\ Bt + 3.15\ Ms + 2.15\ Pl. \quad (8)$$

This is close to the typical mode of a plagioclase-muscovite pseudomorph (Fig. 4c). This result indicates that Na metasomatism, at the hand-specimen scale under conditions where the advective transport rate is only slightly larger than the diffusive transport rate, can form this type of pseudomorph. The sensitivity of mineral modes in the pseudomorph to variations in the magnitude of the Na diffusion coefficient is summarized in Figure 8.

Sillimanite-plagioclase-muscovite pseudomorphs. The association of sillimanite with abundant muscovite and plagioclase in this type of pseudomorph (Figs. 4d and 6) suggests that the sillimanite in the interior of the pseudomorph probably grew after staurolite was completely consumed. Here, the Al supply for sillimanite growth likely came from the breakdown of the paragonite component in muscovite. This suggestion is supported by (1) the textural evidence that the sillimanite appears to cross cut muscovite crystals in the pseudomorph; (2) the field observation that this texture typically occurs upgrade of the last staurolite remnants in the Farmington and Rangeley areas; and (3) texture modeling (Foster 1999) that shows if staurolite reacts in close proximity to sillimanite nuclei, it will produce a sillimanite + biotite pseudomorph with no muscovite. If sillimanite nucleates and grows in a muscovite-rich pseudomorph, such as those shown in Figures 4b and 4c, the local reaction will consume muscovite and produce sillimanite and plagioclase (Fig. 7e) via the reaction:

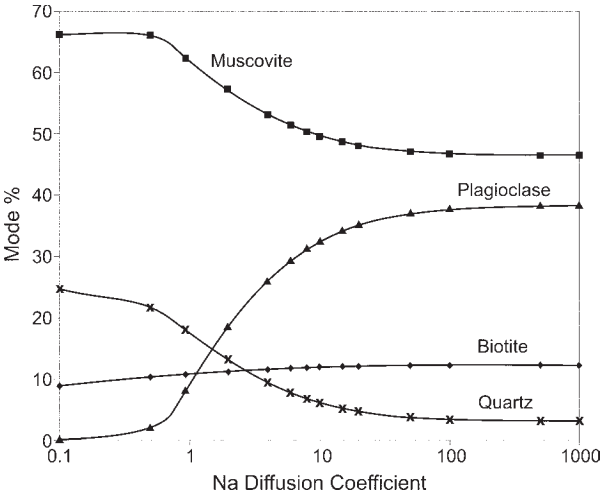

FIGURE 8. Variation of mineral modes in mica pseudomorphs after a staurolite poikiloblast (60% St, 40% Qtz) as a function of the Na diffusion coefficient. A value of 4 produces a plagioclase-muscovite pseudomorph similar to those observed in the Farmington area.

$$0.41\ Ms \rightarrow 0.01\ Pl + 1.0\ Sil + 0.41\ H_2O. \quad (9)$$

This reaction produces sillimanite and plagioclase in a volumetric ratio of about 50:1 and results in a texture similar to that shown in the interior of the pseudomorph (Fig. 4d). Because the sillimanite and plagioclase are present in nearly equal volume in the pseudomorph (Fig. 4d; Table 2), much of the plagioclase in the pseudomorph must predate the sillimanite growth, suggesting that the original staurolite was replaced by a plagioclase-muscovite pseudomorph. The biotite-plagioclase-rich mantle around the pseudomorph suggests that the original staurolite was low in poikilitic quartz requiring that some of the silica used in the staurolite-consuming reaction was derived from quartz in the matrix by a reaction similar to reaction 5. Late sillimanite nucleates and grows in this mantle via reactions (Fig. 7c) such as

$$0.56\ Ms + 0.05\ Pl \rightarrow 1.0\ Sil + 0.48\ Qtz + 0.13\ Bt + 0.43\ H_2O. \quad (10)$$

DISCUSSION

Each of the pseudomorphs modeled preserves subtle evidence of controls during prograde metamorphism. Quartz-muscovite pseudomorphs indicate that the original staurolite contained quartz in excess of that needed for the local staurolite breakdown reaction. These pseudomorphs likely characterize more quartz-rich bulk compositions. In contrast, muscovite pseudomorphs occur in rocks where staurolite contains 20–25% quartz in the poikiloblast requiring that the silica must be transported from the matrix to the pseudomorph during staurolite breakdown. These quartz-consuming reactions result in a zone devoid of quartz—the characteristic biotite-plagioclase-rich mantle region—around the staurolite pseudomorph. Both pseudomorph types represent reaction mechanisms consistent with reaction 2 and do not require migration of any component, except H_2O, beyond the hand-specimen scale. The constituents that diffuse to or from

the muscovite pseudomorphs are produced or consumed by sillimanite-forming reactions that consume muscovite elsewhere in the rock. The staurolite pseudomorph and sillimanite-forming local reactions sum to reaction 1.

Prograde muscovite pseudomorphs after staurolite are found in compositionally similar metapelites with a matrix of biotite, muscovite, quartz, plagioclase, and ilmenite in the sillimanite zone of the adjacent Rangeley-Oquossoc area (Fig. 1; Guidotti 1968, 1970, 1974; Foster 1977, 1981, 1982). In that case, the muscovite pseudomorphs are composed of 60–70% muscovite, 10–15% biotite, 3% plagioclase, 3–5% quartz, and 1–5% ilmenite; these modes are similar to the quartz-muscovite pseudomorph type observed in this study, and it is suggested that they formed by a similar reaction mechanism.

The infiltration of compositionally distinct fluids is recorded in two pseudomorph types from Farmington. Plagioclase-muscovite pseudomorphs could be reproduced only in a system open to Na as well as H_2O at the hand-specimen scale. This result suggests that these types of pseudomorphs develop in a system affected by infiltrating fluids rich in Na. Although the fluids carried other elements, these elements were likely in equilibrium with the mineral assemblage, did not drive reactions, and therefore, their influence was unrecorded (see activity-activity diagram in Dutrow et al. 1999 for equilibrium fluid compositions in similar rocks). Sillimanite-plagioclase-muscovite pseudomorphs appear to result from a two-stage process in which the original staurolite produced a plagioclase-biotite pseudomorph (due to Na infiltration) followed by development of sillimanite after the original staurolite had been completely replaced. Multistage pseudomorph development is also suggested to have formed the tourmaline-rich muscovite pseudomorphs that occur elsewhere in the Farmington quadrangle (Dutrow et al. 1999).

Not all reported plagioclase-rich pseudomorphs after staurolite are indicative of Na metasomatism. For example, the plagioclase-biotite pseudomorphs from the File Lake, Manitoba area (Bailes and McRitchie 1978; Bailes 1980) are produced by the same whole-rock reaction as muscovite-rich pseudomorphs near Rangeley, Maine: Ms + St + Qtz → Sil + Bi + Grt (Bailes, 1980; Guidotti 1968, 1974). Texture modeling has shown that the amount of muscovite in the rock is the critical factor that allows the plagioclase-biotite pseudomorphs to be produced by the same continuous whole-rock reaction that creates muscovite-rich pseudomorphs. The Rangeley, Maine rocks are muscovite-rich (~25% Ms), whereas the File Lake rocks are muscovite-poor (~5% Ms, Figs. 9a and 9b).

When sillimanite nucleates and grows in a rock containing staurolite poikiloblasts in a matrix of muscovite, biotite, plagioclase, and quartz, the material transport constraints im-

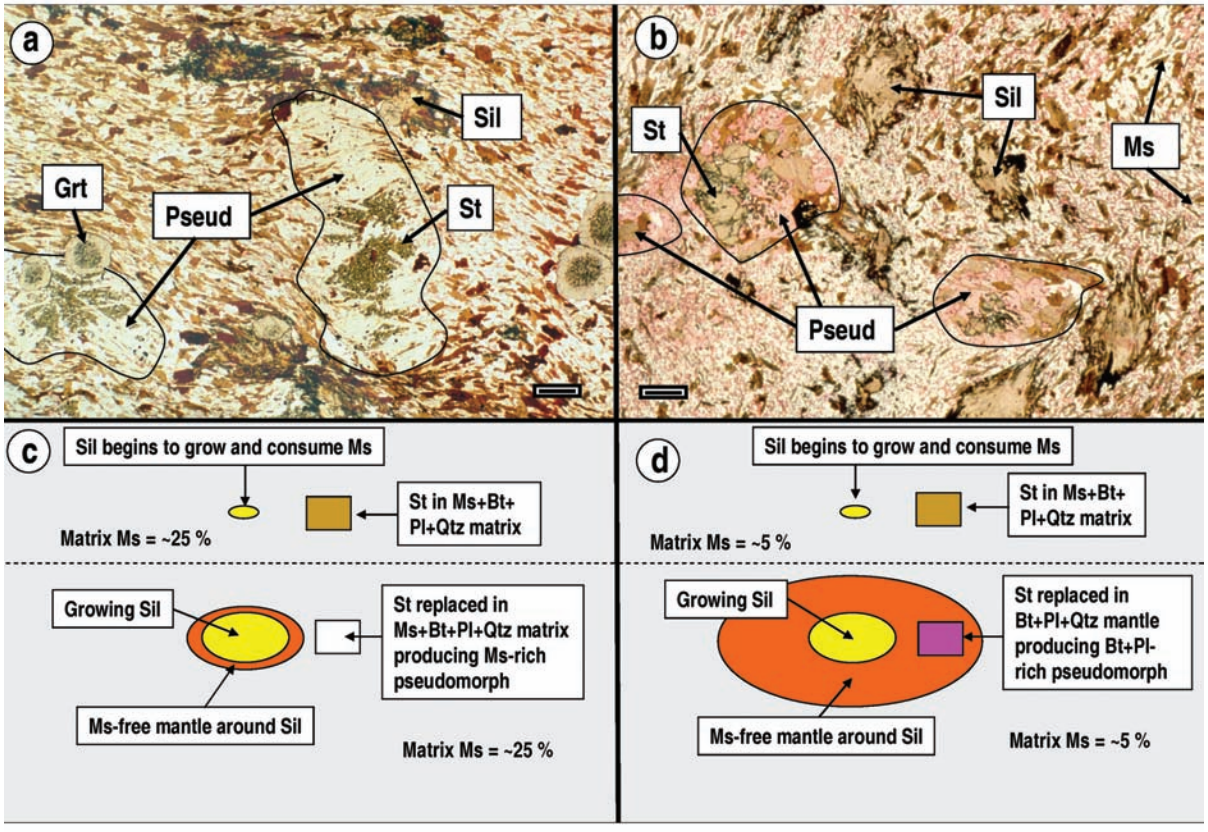

Figure 9. (**a**, **b**) Photomicrographs (plane-polarized light) with plagioclase stained pink showing the difference in modal mineralogy of the pseudomorphs despite the same overall reaction that produced them. Scale bars are 1 mm. (**a**) Muscovite-rich pseudomorph after staurolite from the lower sillimanite zone near Rangeley, Maine. (**b**) Plagioclase-biotite pseudomorphs after staurolite from the sillimanite biotite zone near File Lake, Manitoba. (**c**) Schematic diagram showing the predominant textures that develop in muscovite-rich rocks similar to those at Rangeley. (**d**) Schematic diagram showing the predominant textures that develop in muscovite-poor rocks similar to those at File Lake.

posed by the Gibbs-Duhem equations of the matrix phases in local equilibrium around the growing sillimanite results in the local reaction: Ms + Pl → Sil + Bi + Qtz (Foster 1981, 1982). This reaction produces a muscovite-free mantle around the sillimanite (see Foster 1982 for discussion of variations). Because the amount of muscovite in the File Lake rocks is about 1/5 of that in the Rangeley rocks, the volume of matrix necessary to provide the muscovite needed for the local sillimanite growth reaction is about five times larger at File Lake than at Rangeley. Consequently, most staurolites at File Lake are replaced in muscovite-free local environments although most of the staurolites in Rangeley were replaced in muscovite-bearing local environments (Figs. 9c and 9d).

The presence or absence of muscovite around the reacting staurolite has a profound effect on the staurolite-consuming reaction because of the Gibbs-Duhem constraint on chemical potential gradients in the matrix around the staurolite provided by muscovite. If muscovite is present in the matrix surrounding the porphyroblast, the local staurolite-consuming reaction is St + Qtz → Ms + Bi + Pl (Foster 1981, 1983). If muscovite is absent in the matrix surrounding the porphyroblast, the local staurolite-consuming reaction is St + Qtz → Bi + Pl (Foster 1983). The precise stoichiometry of these reactions depends on the mineral compositions and grain boundary diffusion coefficients. Figure 10 shows the calculated modes for Rangeley and File Lake rocks using the relative diffusion coefficients calculated by Foster (1981), compared to the actual modes measured in rocks from each area. The fact that the calculated modes agree closely with the observed modes at File Lake provides another indication that the Foster (1981) coefficients are valid for a wide variety of compositions in sillimanite grade rocks.

To illustrate the sensitivity of the texture models to the relative diffusion coefficients, test calculations were preformed in which the value for the Al coefficient was varied from 0.1 to 15 while holding the others constant at given values (Table 3, Fig. 11; Foster 1983). For a staurolite poikiloblast (71% St, 29% Qtz) containing one mole of staurolite that reacts in a matrix of biotite, muscovite, plagioclase, quartz, and ilmenite under H_2O-saturated conditions, the minerals most sensitive to the value of the Al coefficient are quartz and muscovite (Fig. 11). In contrast, staurolite, plagioclase, biotite, and ilmenite are insensitive to the choice of the Al relative diffusion coefficients. The bold portions of the muscovite and quartz curves show the range of stoichiometric coefficients that produce muscovite/quartz ratios that are within one standard deviation of the mean of 27 muscovite-rich pseudomorphs from specimen RA66N in the Rangeley, Maine area. The values observed in RA66N are centered near the mean value of the Al coefficient given in Table 3. As might be expected, biotite, plagioclase, and ilmenite are influenced more by variations in the Fe, Na, and Ti relative diffusion coefficients. Variations of the diffusion coefficient of any component within the standard deviations given by Foster (1981) produce relatively small variations in reaction stoichiometry that are similar to those shown in Figure 11.

Although other localities containing muscovite-rich pseudomorphs have been reported in the literature (see Introduction), these studies do not present the necessary information to allow a direct or quantitative comparison. However, they do present suggestions to account for pseudomorph development that include both a single prograde metamorphic event or overprinting metamorphic events. Our studies provide a direct method to evaluate the likely reaction mechanisms responsible for pseudomorphing process thus allowing inferences to be made about metamorphic conditions.

Of the four muscovite-pseudomorph types reported in this study, two are related to local bulk-compositional effects (the amount of poikilitic quartz in staurolite), one type requires fluid infiltration, and the other requires a two-stage process involving fluid infiltration and later mineral growth after a pseudomorph

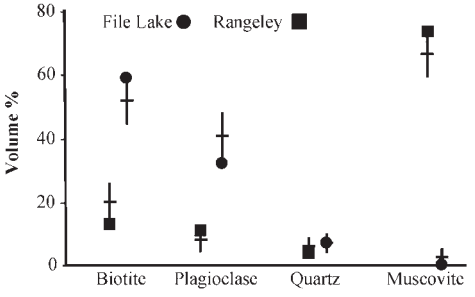

FIGURE 10. Vertical lines with horizontal tick marks show mean and standard deviations of mineral modes in pseudomorphs from the File Lake and Rangeley areas. Circles show modes calculated by texture model using Foster (1981) diffusion coefficients. Note that all model values fall within one standard deviation of observed values.

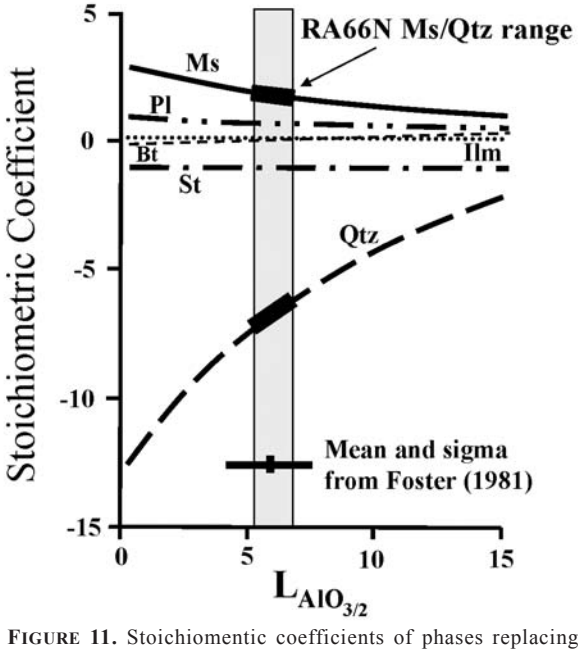

FIGURE 11. Stoichiomentic coefficients of phases replacing poikiloblastic staurolite in a matrix of muscovite, biotite, plagioclase, quartz, and ilmenite plotted as a function of the aluminum diffusion coefficient (Foster 1983). The bold portion of the muscovite and quartz curves show where the quartz to muscovite ratio is within one standard deviation of the observed ratio in Rangeley, Maine rocks. The mean and standard deviation of the aluminum diffusion coefficient calculated by Foster (1981) is also shown. Mineral formulae are given in Foster (1983).

has formed to produce the observed mineralogy. Because each type represents a different reaction mechanism of formation, muscovite-bearing pseudomorphs retain subtle evidence of the metamorphic conditions or controls during prograde development. Guidotti (1968) first recognized the importance of muscovite pseudomorphs after staurolite. This study demonstrates that careful analyses can extend his original studies to determine the details of the processes responsible for their occurrence. These data provide additional insights into the prograde conditions within the Farmington area of Maine that previously have gone unrecognized, and underscore the utility of pseudomorphs and their subtle mineralogical variations in unraveling metamorphism as pointed out originally by Guidotti (e.g., 1968).

Acknowledgments

Funding for this research was provided by DOE EPSCoR/BES grant DE-FG02-03ER-46041 to B. Dutrow, by the National Science Foundation EAR-9814372 to Foster and EAR9814418 to B. Dutrow, and by the Shreveport Geological Society, Shell Oil Company, and the LSU Department of Geology and Geophysics to Whittington. X. Xie is thanked for assistance with imaging and chemical analyses and D. Henry for valuable discussions throughout this research. M.J. Holdaway is gratefully acknowledged for introducing Dutrow to the area and for inspiring this work. John Brady, Ed Grew, and an anonymous reviewer provided helpful comments that greatly improved (and lengthened) the manuscript. Our special appreciation to Charlie, who guided us through the rocks and their stories, and who will always be an inspiration.

References cited

Bailes, A.H. (1980) Geology of the File Lake Area. Manitoba Department of Energy and Mines, Mineral Resource Division Geological Report (Winnipeg), 78-1, 134 p.

Bailes, A.H. and McRitchie, W.D. (1978) The transition from low to high grade metamorphism in the Kisseynew sedimentary gneiss belt, Manitoba. Metamorphism in the Canadian Shield. Geological Survey of Canada, Paper 78-10, p. 155–178.

Brady, J.B., Markley, M.J., Schumacher, J.C., Cheney, J.T., and Bianciardi, G.A. (2004) Aragonite pseudomorphs in high-pressure marbles of Syros, Greece. Journal of Structural Geology, 26, 3–9.

Cesare, B. (1999a) Multi-stage pseudomorphic replacement of garnet during polymetamorphism: 1. Microstructures and their interpretation. Journal of Metamorphic Geology, 17, 723–734.

——— (1999b) Multi-stage pseudomorphic replacement of garnet during polymetamorphism: 2. Algebraic analysis of mineral assemblages. Journal of Metamorphic Geology, 17, 735–746.

Collier, J.B. and Plimer, I.R. (2002) Supergene clinobisvanite pseudomorphs after supergene dreyerite from Lively's Mine, Arkaroola, South Australia. Neues Jahrbuch für Mineralogie-Monatshefte, 9, 401–410.

DeYoreo, J.J., Lux, D.R., and Guidotti, C.V. (1989) A thermal model for Carboniferous metamorphism near the Sebago Batholith in western Maine. In R.D. Tucker and R.G. Marvinney, Eds., Igneous and metamorphic geology. Studies in Maine Geology, 3, 19–34.

Dutrow, B.L. (1985) A staurolite trilogy: Part III. Evidence for multiple metamorphic episodes in the Farmington quadrangle, Maine. Ph.D. dissertation, Southern Methodist University, Dallas, Texas.

Dutrow, B.L., Foster, C.T., Jr., and Henry, D.J. (1999) Tourmaline-rich pseudomorphs in sillimanite zone metapelites: Demarcation of an infiltration front. American Mineralogist, 84, 794–805.

Ferry, J.M. (2000) Patterns of mineral occurrence in metamorphic rocks. American Mineralogist, 85, 1573–1588.

Fisher, G.W. (1977) Nonequilibrium thermodynamics in metamorphism. NATO ASI Series, Conference Series C: Mathematical and Physical Sciences, 30, 381–403. Reidel, Dordrecht, Netherlands.

Foster, C.T., Jr. (1977) Mass transfer in sillimanite-bearing pelitic schists near Rangeley, Maine. American Mineralogist, 62, 727–746.

——— (1981) A thermodynamic model of mineral segregations in the lower sillimanite zone near Rangeley, Maine. American Mineralogist, 66, 260–277.

——— (1982) Textural variations of sillimanite segregations. Canadian Mineralogist, 20, 379–392.

——— (1983) Thermodynamic models of biotite pseudomorphs after staurolite. American Mineralogist, 68, 389–397.

——— (1986) Thermodynamic models of reactions involving garnet in a sillimanite/staurolite schist. Mineralogical Magazine, 50, 427–439.

——— (1990) Control of material transport and reaction mechanisms by metastable mineral assemblages: An example involving kyanite, sillimanite, muscovite and quartz. In R.J. Spencer and I-M. Chou, Eds., Fluid-Mineral Interactions. Geochemical Special Publication No. 2, 121–132.

——— (1991) The role of biotite as a catalyst in reaction mechanisms that form sillimanite. Canadian Mineralogist, 29, 943–963.

——— (1993) Seg93: A program to model metamorphic textures. Geological Society of America Abstracts with Program, 25, no. 7, A264.

——— (1999) Forward modeling of metamorphic textures. Canadian Mineralogist (Kretz Volume), 37, 415–429.

Grew, E.S. and Day, H.W. (1972) Staurolite, kyanite, and sillimanite from the Narragansett Basin of Rhode Island. U.S. Geological Survey Professional Paper 800-D, D151–D157.

Guidotti, C.V. (1968) Prograde muscovite pseudomorphs after staurolite in the Rangeley-Oquossoc areas, Maine. American Mineralogist, 53, 1368–1376.

——— (1970) The mineralogy and petrology of the transition from the lower to upper sillimanite zone in the Oquossoc area, Maine. Journal of Petrology, 11, 277–336.

——— (1973) Compositional variation of muscovite as a function of metamorphic grade and assemblage in metapelites from northwest Maine. Contributions to Mineralogy and Petrology, 42, 33–42.

——— (1974) Transition from staurolite to sillimanite zone, Rangeley quadrangle, Maine. Geological Society of America Bulletin, 85, 475–490.

——— (1989) Metamorphism in Maine: An overview. Maine Geological Survey, Studies in Maine Geology, 3, 1–17.

Guidotti, C.V. and Holdaway, M.J. (1993) Petrology and field relations of successive metamorphic events in pelites of west-central Maine. In J.T. Cheney and J.C. Hepburn, Eds., Field trip guidebook for the northeastern United States. Geology Department, University of Massachusetts, 67, 1, 1–26.

Guidotti, C.V. and Johnson, S.E. (2002) Pseudomorphs and associated microstructures of western Maine, U.S.A. Journal of Structural Geology, 24, 1139–1156.

Guidotti, C.V., Cheney, J.T., Foster, C.T., Jr., Hames, W.E., Henry, D.J., Kinner, D.A., and Lux, D.R. (1996) Polymetamorphism in western Maine; mineralogic, petrologic and textural manifestations and regional geologic implications. In M.R. Van Baalen, Ed., Guidebook to field trips in northern New Hampshire and adjacent regions of Maine and Vermont, 171–202. Harvard Printing and Publication Services, Cambridge, Massachusetts.

Henry, D.J., Guidotti, C.V., and Thomson, J.A. (2005) The Ti-saturation surface for low-to-medium pressure metapelitic biotites: Implications for geothermometry and Ti-substitution mechanisms. American Mineralogist, 90, 316–328.

Holdaway, M.J., Guidotti, C.V., Novak, J.M., and Henry, W.E. (1982) Polymetamorphism in medium- to high-grade pelitic metamorphic rocks, west-central Maine. Geological Society of America Bulletin, 93, 572–584.

Holdaway, M.J., Dutrow, B.L., and Hinton, R.W. (1988) Devonian and Carboniferous metamorphism in west-central Maine: The muscovite-almandine geobarometer and the staurolite problem revisited. American Mineralogist, 73, 20–47.

Johnson, J. and Norton, D. (1985) Theoretical prediction of hydrothermal conditions and chemical equilibria during skarn formation in porphyry copper systems. Economic Geology, 80, 1797–1823.

Kretz, R. (1983) Symbols for rock-forming minerals. American Mineralogist, 68, 277–279.

Kwak, T.A.P. (1974) Natural staurolite breakdown reactions at moderate to high pressures. Contributions to Mineralogy and Petrology, 44, 57–80.

Moench, R.H. and Pankiwskyj, K.A. (1988) Definition, problems, and reinterpretation of early premetamorphic faults in western Maine and northeastern New Hampshire. In R.D. Tucker and R.G. Marvinney, Eds., Structure and stratigraphy. Studies in Maine Geology, p. 35–50.

Moench, R.H. and Zartman, R.E. (1976) Chronology and styles of multiple deformation, plutonism, and polymetamorphism in the Merrimack Synclinorium of western Maine. Geological Society of America Memoir, Studies in New England geology; northern New England, 146, p. 203–238.

Novák, M., Černý, P., Cempírek, J., Šrein, V., and Filip, J. (2004) Ferrotapiolite as a pseudomorph of stibiotantalite from the Latošvičky lepidolite pegmatite, Czech Republic; an example of hydrothermal alteration at constant Ta/(Ta+Nb). Canadian Mineralogist, 42(4), 1117–1128.

Pankiwskyj, K.A., Ludman, A., Griffen, J.R., and Berry, A.B.N. (1976) Stratigraphic relationships on the southwest limb of the Merrimack synclinorium in central and west central Maine. In P.C. Lyons and A.H. Brownlow, Eds., Studies in New England Geology. Geological Society of America Memoirs, 146, 263–280.

Rasband, W.S. (1997–2007) ImageJ. U.S. National Institutes of Health, Bethesda, Maryland. Accessed via http://rsb.info.nih.gov/ij/.

Whittington, J. (2006) Muscovite pseudomorphs after staurolite as a record of fluid infiltration during prograde metamorphism, 119 p. M.S. thesis, Louisiana State University, Baton Rouge, Louisiana.

Manuscript received February 22, 2007
Manuscript accepted September 18, 2007
Manuscript handled by Edward Grew

Appendix 1: Additional analytical methods

Cathodoluminescene (CL) images are used to detect subtle mineral zoning, alteration products along mineral edges, sealed fractures in quartz, and to highlight small mineral grains. CL images of polished thin sections coated with carbon were collected using an Oxford Instruments PA[10] CL detector fitted to the JEOL SEM with a working distance of 13 mm. The hemispherical opening of the collection device allows for a magnification of 130× (0.2816 pixels/μm), making the final image size 0.74 mm in diameter. The SEM operated with an accelerating potential of 20 kV with a beam current of 20–30 nA. Because pseudomorphs are typically 4.0–7.0 mm in size and because the size of the CL collection area is limited, a series of images were collected on a grid to capture the entire pseudomorph. The images were then combined using Adobe Photoshop to display the pseudomorph, mantle, and surrounding matrix.

Quantitative chemical compositions of selected minerals were obtained by wavelength-dispersive spectrometry (WDS) using the JEOL 733 electron microprobe at LSU. Plagioclase was analyzed for the elements Si, Al, K, Na, Ca, and Ba; biotite and muscovite for Si, Al, Fe, Mg, Cr, Ti, Mn, K, Na, Ca, Ba, F, and Cl. A series of well-characterized natural and synthetic silicates were used as standards. Analyses were performed at an accelerating potential of 15 kV, a beam current of ~10 nA, using a 1–2 μm focused electron beam for plagioclase and a 10 μm beam for micas. Two to five spot analyses per grain were collected for counting times of 30–60 s per element in biotite and muscovite, and 20–40 s in plagioclase. On the basis of replicate analyses of several secondary standards, analytical precision associated with counting statistics for selected oxides is estimated to be near 1 relative wt%. Traverses of plagioclase grains within the pseudomorphs, mantle regions, and matrix of four samples (164, 172a, and 183a, 147) were done to identify any chemical zoning.

Stoichiometric calculations for plagioclase were normalized on the basis of eight O atoms; biotite and muscovite were normalized on the basis of 22 O atoms. Staurolite data were normalized to Si + Al = 25.43. Quartz grains from two samples were analyzed with spot traverses to detect trace elements associated with CL zoning. To detect Al^{3+} and Ti^{4+} at trace levels, the analyses required high currents (100 nA) with long count times (30–40 s for Si, 110–140 s for Al and Ti).

Appendix 2: Reaction modeling calculation details

The texture modeling used in this paper is based on the irreversible thermodynamic approach of Fisher (1977). It utilizes the concept that when a mineral grows or is consumed in a matrix of other minerals under local equilibrium conditions, there is a unique set of local reactions that take place that depend on the mineral compositions, mineral modes, thermodynamic diffusion coefficients, and the amount of the "central" mineral that grows or is consumed. The procedure summarized here is derived from first principles in excruciating detail in Foster (1981) and readers are referred there for a more in-depth analysis.

The constraints that allow calculation of the local reaction when one mole of staurolite is consumed while surrounded by a matrix of biotite, muscovite, plagioclase, and quartz under H_2O-saturated conditions (reaction 2) is shown in Figure A1. The first four equations are derived from the Gibbs-Duhem relations for the matrix phases biotite, muscovite, plagioclase and quartz, respectively. The next eight equations are conservation equations that relate the amount of each component produced or consumed by the local reaction to the integral of the fluxes over a closed surface surrounding the reaction. The last equation is a conservation equation that relates the amount of H_2O produced or consumed by the reacting minerals to the amount of water produced or consumed by the reaction. The first eight terms ($\nabla\mu_i \cdot A$) of the solution matrix gives the relative chemical potential gradients of each component. The next five terms (R_j) in the solution matrix gives the number of moles of biotite, muscovite, plagioclase, quartz, and water that are produced or consumed when one mole of staurolite is replaced in a matrix of biotite, muscovite, plagioclase, and quartz under H_2O-saturated conditions. The total amount of each component diffusing in or out of the surface surrounding the reaction volume when one mole of staurolite is consumed can be obtained by multiplying $-\nabla\mu_i \cdot A$ by the thermodynamic diffusion coefficient (L_i).

Using the mineral compositions in Table 1 and the relative thermodynamic diffusion coefficients in Table 3 produces a result of –0.986, 1.267, 0.078, –0.966, 0.000, 3.306, 0.923, 0.055 for the chemical potential terms of FeO, $NaO_{1/2}$, MgO, $AlO_{3/2}$, SiO_2, $KO_{1/2}$, CaO, and TiO_2, respectively, and 0.55, 3.57, 0.71, –6.64, –2.43 for the amounts of biotite, muscovite, plagioclase, quartz and water produced (+) or consumed (–) when one mole of staurolite reacts. These are the values of the stoichiometric coefficients given for reaction 2 in the text. Multiplying the negative of the chemical potential terms times the relative thermodynamic diffusion coefficients (Table 3) give the moles of each component supplied (–) or removed (+) by diffusion through the matrix to balance this reaction: 2.59 FeO, –1.17 $NaO_{1/2}$, –0.14 MgO, 5.68 $AlO_{3/2}$, 0.00 SiO_2, –3.31 $KO_{1/2}$, –0.16 CaO, –0.02 TiO_2 (see Fig. 7a).

The only solid phase that is consumed by reaction 2 is quartz. If the staurolite has more than 25.5% quartz inclusions, all the quartz consumed by reaction 2 can be provided by the quartz in the poikiloblast and a pseudomorph consisting on biotite, muscovite, plagioclase, and quartz will result. The volume of quartz remaining in the pseudomorph is the amount by which the precentage quartz in the poikiloblast exceeds 25.5%. If there is not enough quartz in the poikiloblast to provide all of the quartz required for reaction 2, the necessary silica has to come from consumption of matrix quartz and the pseudomorph will be quartz-free. This means that after a small amount of reaction the staurolite consumption reaction will be taking place inside the quartz-free pseudomorph and the material transport will no longer be constrained by the quartz Gibbs-Duhem equation. This situation can be solved by removing the Gibbs-Duhem coefficients in row 4 of the matrix shown in Figure A1 and replacing them with zeros in all columns of row 4 except for a 1 in column 12. This sets up an equation that makes quartz in the reaction equal to the value in the fourth row of the right hand side column matrix.

In the case of reaction 3, the fourth row of the right hand side column matrix will be zero ($R_Q = 0$) because there is no poikilitic quartz in the porphyroblast; in the case of reaction 4 the fourth row of the right hand side matrix will be –4.85 ($R_Q =$

$$\begin{bmatrix} \upsilon_{Fe}^{B} & \upsilon_{Na}^{B} & \upsilon_{Mg}^{B} & \upsilon_{Al}^{B} & \upsilon_{Si}^{B} & \upsilon_{K}^{B} & \upsilon_{Ca}^{B} & \upsilon_{Ti}^{B} & 0 & 0 & 0 & 0 & 0 \\ \upsilon_{Fe}^{M} & \upsilon_{Na}^{M} & \upsilon_{Mg}^{M} & \upsilon_{Al}^{M} & \upsilon_{Si}^{M} & \upsilon_{K}^{M} & \upsilon_{Ca}^{M} & \upsilon_{Ti}^{M} & 0 & 0 & 0 & 0 & 0 \\ \upsilon_{Fe}^{P} & \upsilon_{Na}^{P} & \upsilon_{Mg}^{P} & \upsilon_{Al}^{P} & \upsilon_{Si}^{P} & \upsilon_{K}^{P} & \upsilon_{Ca}^{P} & \upsilon_{Ti}^{P} & 0 & 0 & 0 & 0 & 0 \\ \upsilon_{Fe}^{Q} & \upsilon_{Na}^{Q} & \upsilon_{Mg}^{Q} & \upsilon_{Al}^{Q} & \upsilon_{Si}^{Q} & \upsilon_{K}^{Q} & \upsilon_{Ca}^{Q} & \upsilon_{Ti}^{Q} & 0 & 0 & 0 & 0 & 0 \\ L_{Fe} & 0 & 0 & 0 & 0 & 0 & 0 & 0 & \upsilon_{Fe}^{B} & \upsilon_{Fe}^{M} & \upsilon_{Fe}^{P} & \upsilon_{Fe}^{Q} & 0 \\ 0 & L_{Na} & 0 & 0 & 0 & 0 & 0 & 0 & \upsilon_{Na}^{B} & \upsilon_{Na}^{M} & \upsilon_{Na}^{P} & \upsilon_{Na}^{Q} & 0 \\ 0 & 0 & L_{Mg} & 0 & 0 & 0 & 0 & 0 & \upsilon_{Mg}^{B} & \upsilon_{Mg}^{M} & \upsilon_{Mg}^{P} & \upsilon_{Mg}^{Q} & 0 \\ 0 & 0 & 0 & L_{Al} & 0 & 0 & 0 & 0 & \upsilon_{Al}^{B} & \upsilon_{Al}^{M} & \upsilon_{Al}^{P} & \upsilon_{Al}^{Q} & 0 \\ 0 & 0 & 0 & 0 & L_{Si} & 0 & 0 & 0 & \upsilon_{Si}^{B} & \upsilon_{Si}^{M} & \upsilon_{Si}^{P} & \upsilon_{Si}^{Q} & 0 \\ 0 & 0 & 0 & 0 & 0 & L_{K} & 0 & 0 & \upsilon_{K}^{B} & \upsilon_{K}^{M} & \upsilon_{K}^{P} & \upsilon_{K}^{Q} & 0 \\ 0 & 0 & 0 & 0 & 0 & 0 & L_{Ca} & 0 & \upsilon_{Ca}^{B} & \upsilon_{Ca}^{M} & \upsilon_{Ca}^{P} & \upsilon_{Ca}^{Q} & 0 \\ 0 & 0 & 0 & 0 & 0 & 0 & 0 & L_{Ti} & \upsilon_{Ti}^{B} & \upsilon_{Ti}^{M} & \upsilon_{Ti}^{P} & \upsilon_{Ti}^{Q} & 0 \\ 0 & 0 & 0 & 0 & 0 & 0 & 0 & 0 & \upsilon_{H2O}^{B} & \upsilon_{H2O}^{M} & \upsilon_{H2O}^{P} & \upsilon_{H2O}^{Q} & \upsilon_{H2O}^{W} \end{bmatrix} \bullet \begin{bmatrix} \nabla\mu_{Fe}\bullet A \\ \nabla\mu_{Na}\bullet A \\ \nabla\mu_{Mg}\bullet A \\ \nabla\mu_{Al}\bullet A \\ \nabla\mu_{Si}\bullet A \\ \nabla\mu_{K}\bullet A \\ \nabla\mu_{Ca}\bullet A \\ \nabla\mu_{Ti}\bullet A \\ R_B \\ R_M \\ R_P \\ R_Q \\ R_W \end{bmatrix} = \begin{bmatrix} 0 \\ 0 \\ 0 \\ 0 \\ -\upsilon_{Fe}^{St} \\ -\upsilon_{Na}^{St} \\ -\upsilon_{Mg}^{St} \\ -\upsilon_{Al}^{St} \\ -\upsilon_{Si}^{St} \\ -\upsilon_{K}^{St} \\ -\upsilon_{Ca}^{St} \\ -\upsilon_{Ti}^{St} \\ -\upsilon_{H2O}^{St} \end{bmatrix}$$

Appendix Figure 1. Matrix equation to solve for reaction 2. R_j is reaction coefficient of phase j, ∇_i is the chemical potential gradient of component i, υ_i^j is stoichiometric coefficient of component i in phase j, A is the area of a closed surface surrounding the reaction volume where the chemical potential gradients are measured, and L_i is the relative thermodynamic diffusion coefficient for component i. Fe, Na, Mg, Al, Si, K, Ca, and Ti stand for the components FeO, $NaO_{1/2}$, MgO, $AlO_{3/2}$, SiO_2, $KO_{1/2}$, CaO, and TiO_2, respectively. B, M, P, Q, W, St indicate biotite, muscovite, plagioclase, quartz, water, and staurolite, respectively.

–4.85) because the poikiloblast has 20% quartz, which will be consumed by the reaction, requiring 4.85 fewer moles of SiO_2 to diffuse through the pseudomorph to react with one mole of staurolite. The solution matrix for reaction 3 is –1.122, 0.387, –0.066, –1.346, 0.513, 2.927, –0.381, –0.017 for the chemical potential terms of FeO, $NaO_{1/2}$, MgO, $AlO_{3/2}$, SiO_2, $KO_{1/2}$, CaO and TiO_2, respectively, and 0.29, 3.38, –0.29, 0.00, and 1.98, for R_B, R_M, R_P, R_Q, and R_W, respectively.

The solution matrix for reaction 4 is –1.023, 1.030, 0.039, –1.069, 0.139, 3.204, 0. 571, 0.036 for the chemical potential terms of FeO, $NaO_{1/2}$, MgO, $AlO_{3/2}$, SiO_2, $KO_{1/2}$, CaO and TiO_2, respectively, and 0.48, 3.52, 0.44, –4.85, and –2.31, for R_B, R_M, R_P, R_Q, and R_W, respectively. The reason that the reaction stoichiometry and chemical potential gradients change is that reaction 4 requires fewer moles of SiO_2 to be supplied by diffusion through the pseudomorph, substantially lowering the chemical potential gradient of SiO_2 in the pseudomorph, which affects all the other chemical potential gradients through the Gibbs-Duhem relations of biotite, muscovite, and plagioclase. The amount of each component supplied (–) or removed (+) by diffusion through the biotite, muscovite, plagioclase pseudomorph when one mole of staurolite reacts is 2.95 FeO, –0.36 $NaO_{1/2}$, 0.12 MgO, 7.92 $AlO_{3/2}$, –2.57 SiO_2, –2.92 $KO_{1/2}$, 0.06 CaO, 0.01 TiO_2 for reaction 3, and 2.69 FeO, –0.96 $NaO_{1/2}$, –0.07 MgO, 6.29 $AlO_{3/2}$, –0.69 SiO_2, –3.20 $KO_{1/2}$, –0.08 CaO –0.01 TiO_2 for reaction 4.

The chemical potential gradients in the quartz-bearing matrix around the pseudomorph, and within the quartz-free pseudomorphs produced by a reaction like 3, 4, and 6 are different; this causes quartz-consuming reactions to proceed out into the matrix, consuming and producing components to account for the difference in the fluxes between the pseudomorph and the matrix. The amount of each component produced or consumed by the quartz-consuming reaction can be calculated by subtracting the amount of material supplied or removed through the pseudomorph from the amount of material supplied or removed though the matrix. For example, reaction 5 consumes (–) or produces (+) –0.35 FeO, –0.82 $NaO_{1/2}$, –0.26 MgO, –2.24 $AlO_{3/2}$, 2.57 SiO_2, –0.38 $KO_{1/2}$,–0.22 CaO, and –0.03 TiO_2.